

# Crystal and magnetic structures of $R_2\text{Ni}_2\text{In}$ compounds ( $R = \text{Tb}$ and $\text{Ho}$ )

Stanisław Baran,<sup>1,\*</sup> Aleksandra Deptuch,<sup>2</sup> Andreas Hoser,<sup>3</sup>  
Bogusław Penc,<sup>1</sup> Janusz Przewoźnik,<sup>4</sup> and Andrzej Szytuła<sup>1</sup>

<sup>1</sup>*M. Smoluchowski Institute of Physics, Jagiellonian University,  
prof. Stanisława Łojasiewicza 11, PL-30-348 Kraków, Poland*

<sup>2</sup>*Institute of Nuclear Physics Polish Academy of Sciences, Radzikowskiego 152, PL-31-342 Kraków, Poland*

<sup>3</sup>*Helmholtz-Zentrum Berlin für Materialien und Energie GmbH,  
Hahn-Meitner Platz 1, D-14109, Berlin, Germany*

<sup>4</sup>*AGH University of Science and Technology, Faculty of Physics and Applied Computer Science,  
Department of Solid State Physics, Al. Mickiewicza 30, PL-30-059 Kraków, Poland*

(Dated: July 18, 2022)

Crystal and magnetic structures of  $R_2\text{Ni}_2\text{In}$  ( $R = \text{Tb}$  and  $\text{Ho}$ ) have been studied by powder neutron diffraction at low temperatures. The compounds crystallize in an orthorhombic crystal structure of the  $\text{Mn}_2\text{AlB}_2$ -type. At low temperatures, the magnetic moments localized solely on the rare earth atoms form antiferromagnetic structures. The Tb magnetic moments, equal to  $8.65(6) \mu_B$  and parallel to the  $c$ -axis, form a collinear magnetic structure described by the propagation vector  $\mathbf{k} = [\frac{1}{2}, \frac{1}{2}, \frac{1}{2}]$ . This magnetic structure is stable up to the Néel temperature equal to 40 K. For  $\text{Ho}_2\text{Ni}_2\text{In}$  a complex, temperature-dependent magnetic structure is detected. In the temperature range 3.5–8.6 K, an incommensurate magnetic structure, described by the propagation vector  $\mathbf{k}_1 = [0.76, 0, 0.52]$  is observed, while in the temperature interval 2.2–3.1 K the magnetic order is described by two propagation vectors, namely,  $\mathbf{k}_2 = [\frac{5}{6}, 0.16, \frac{1}{2}]$  and its third harmonics  $3\mathbf{k}_2 = [\frac{5}{2}, 0.48, \frac{3}{2}]$ . Below 2 K, a coexistence of all magnetic structures detected at higher temperatures is observed. For all magnetic phases, the Ho magnetic moments are parallel to the  $c$ -axis. The low temperature heat capacity data confirm a first order transition near 3 K.

## I. INTRODUCTION

There is a strong interest in the development of novel magnetically ordered materials with unconventional properties. The  $R_2\text{Ni}_2\text{In}$  compounds crystallize in the orthorhombic crystal structure (space group  $Cmmm$ ) [1]. Magnetic and specific heat measurements indicate that the  $R_2\text{Ni}_2\text{In}$  ( $R = \text{Gd-Tm}$ ) compounds are antiferromagnets with the Néel temperatures between 5 K ( $R = \text{Tm}$ ) and 40 K ( $R = \text{Tb}$ ) [2]. In all compounds, except  $R = \text{Ho}$ , the magnetic order is stable in a broad temperature range between 1.9 K and a corresponding Néel temperature. For  $\text{Ho}_2\text{Ni}_2\text{In}$ , below the Néel temperature of 9 K, an additional phase transition at  $T_t$  equal 3.5 K (dc magnetic data) or 3.3 K (ac magnetic data and heat capacity data) is observed. The more recent paper reports  $T_N = 10.5$  K and  $T_t = 5.5$  K [3]. The antiferromagnetic order is confirmed by the neutron diffraction data for  $R = \text{Tb}$  [4] as well as Er and Tm [5]. The magnetic structure is described by the propagation vectors  $\mathbf{k} = [\frac{1}{2}, \frac{1}{2}, \frac{1}{2}]$  for  $R = \text{Tb}$  and  $[\frac{1}{2}, 0, \frac{1}{2}]$  for Er and Tm. The magnetic moments are found to be localized solely on the rare earth atoms. They form collinear magnetic structure and are parallel to the  $c$ -axis for Tb and  $b$ -axis for Er and Tm.

In order to deeper understand magnetic properties of  $R_2\text{Ni}_2\text{In}$  ( $R$  - rare earth element), we have performed new neutron diffraction measurements for  $R_2\text{Ni}_2\text{In}$  ( $R = \text{Tb}, \text{Ho}$ ). Although, the magnetic structure of  $\text{Tb}_2\text{Ni}_2\text{In}$

has already been reported [4], the previous data have been collected for the sample containing only 10 wt % of  $\text{Tb}_2\text{Ni}_2\text{In}$ . In the current work we report the results obtained for a new sample consisting of  $\text{Tb}_2\text{Ni}_2\text{In}$  in its most part. In addition, we report for the first time the magnetic structure in  $\text{Ho}_2\text{Ni}_2\text{In}$ . The neutron diffraction data for  $\text{Ho}_2\text{Ni}_2\text{In}$  are supported by heat capacity measurements.

## II. EXPERIMENTAL DETAILS

The samples of  $R_2\text{Ni}_2\text{In}$  ( $R = \text{Tb}$  and  $\text{Ho}$ ) have been prepared by arc melting of  $R$ , Ni and In (all with purity at least 99.9 wt %) taken in the atomic ratio of 2:2:1. The melting has been performed under a Ti-gettered Ar atmosphere. The obtained ingots have been turned over and remelted four times in order to get homogeneous distribution of components. The samples have been homogenized in an evacuated quartz-tube at 873 K for one month, followed by cold water quenching.

The samples' quality has been checked by X-ray powder diffraction at room temperature (PANalytical X'Pert diffractometer with  $\text{CuK}\alpha$  radiation).

Neutron diffraction patterns have been collected in the temperature range from 1.55 up to 60 K on the E6 diffractometer at the Helmholtz-Zentrum Berlin für Materialien in Energie GmbH. The incident neutron wavelength was 2.4315 Å. For Rietveld analysis of the X-ray and neutron diffraction patterns the computer program FullProf has been utilized [6], while for symmetry analysis the computer program BasIreps, which is distributed together

\* stanislaw.baran@uj.edu.pl

with FullProf, has been used.

Heat capacity study have been carried out by a two-tau relaxation method in the temperature range 1.8-12 K using HC option of the Quantum Design PPMS platform.

### III. RESULTS

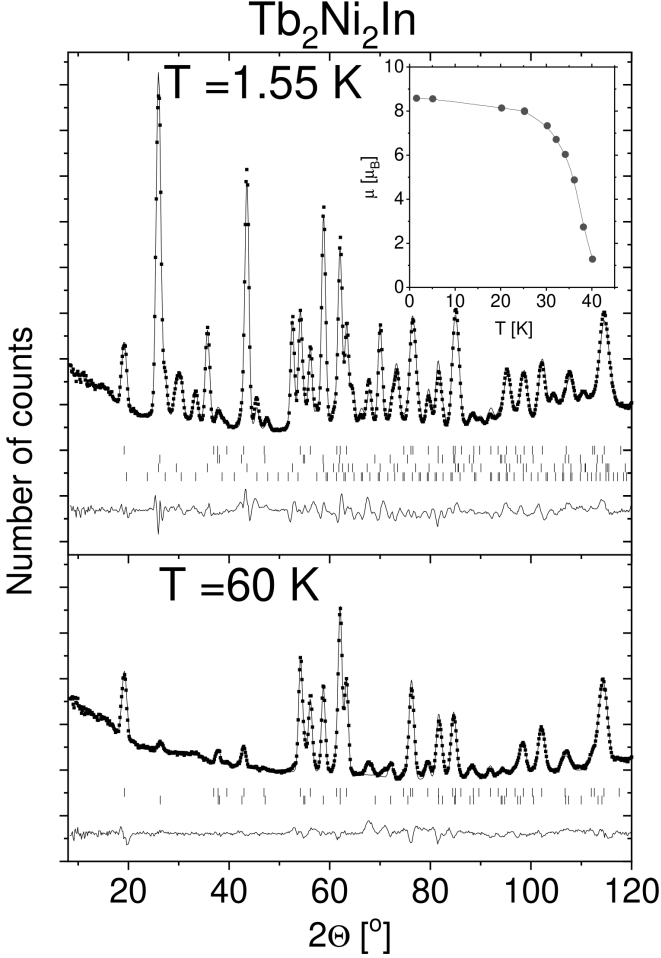


FIG. 1. Neutron diffraction patterns of  $\text{Tb}_2\text{Ni}_2\text{In}$  collected at 1.55 and 60 K. In both patterns the squares represent experimental points. The solid lines are the calculated profiles for the crystal and magnetic structure models (as is described in text) and difference between the observed and calculated intensities (at the bottom of each diagram). The vertical bars indicate the positions of nuclear (first top and third rows) and magnetic (second and fourth row) peaks for  $\text{Tb}_2\text{Ni}_2\text{In}$  and  $\text{Tb}_2\text{Ni}_{1.78}\text{In}$ , respectively. The insert shows the temperature dependence of the Tb magnetic moment.

Analysis of the X-ray diffraction and neutron patterns indicate 82 wt % of  $\text{Tb}_2\text{Ni}_2\text{In}$  and 18 wt % of  $\text{Tb}_2\text{Ni}_{1.78}\text{In}$  for the Tb-based sample and 95.4(3) wt % of  $\text{Ho}_2\text{Ni}_2\text{In}$  and 4.6(3) wt % of  $\text{HoNi}_2$  for the Ho-based sample (see Figures 1a and 2a).

TABLE I. Crystal structure parameters of  $\text{Tb}_2\text{Ni}_2\text{In}$  together with residuals for profile and integrated intensities determined from the neutron diffraction data.

$T$ [K]	60	1.55
$a$ [Å]	3.913(1)	3.910(1)
$b$ [Å]	14.135(2)	14.125(3)
$c$ [Å]	3.691(1)	3.692(1)
$V$ [Å <sup>3</sup> ]	204.15(14)	203.90(16)
$y_{\text{Tb}}$	0.3647(2)	0.3632(3)
$y_{\text{Ni}}$	0.1984(3)	0.1986(3)
$R_{\text{Bragg}}$ [%]	6.2	6.6
$R_f$ [%]	5.0	5.8

TABLE II. Crystal structure parameters of  $\text{Ho}_2\text{Ni}_2\text{In}$  together with residuals for profile and integrated intensities determined from the neutron diffraction data.

$T$ [K]	20.2	3.7	2.5	1.5
$a$ [Å]	3.9178(5)	3.9119(9)	3.9117(8)	3.9122(9)
$b$ [Å]	14.202(2)	14.184(3)	14.184(3)	14.184(3)
$c$ [Å]	3.6715(4)	3.6648(8)	3.6660(7)	3.6652(8)
$V$ [Å <sup>3</sup> ]	204.29(2)	203.34(8)	203.40(7)	203.38(7)
$y_{\text{Ho}}$	0.3639(4)	0.3636(6)	0.3639(6)	0.3644(6)
$y_{\text{Ni}}$	0.1981(4)	0.1972(8)	0.1969(8)	0.1975(7)
$R_{\text{Bragg}}$ [%]	3.4	5.1	4.9	5.3
$R_f$ [%]	2.8	3.6	3.0	3.2

The 2:2:1 compounds crystallize in the orthorhombic crystal structure of the  $\text{Mn}_2\text{AlB}_2$ -type (space group  $Cmmm$ ). The atoms occupy the following Wyckoff sites:  $R$  at  $4j$  ( $0, y_R, \frac{1}{2}$ ),  $\text{Ni}$  at  $4i$  ( $0, y_{\text{Ni}}, 0$ ) and  $\text{In}$  at  $2a$  ( $0, 0, 0$ ). The crystal structure of  $\text{Ho}_2\text{Ni}_2\text{In}$  is shown in Figure 3 together with distances between the  $\text{Ho}1$  atom and its nearest neighbours. The refined crystal structure parameters at different temperatures are listed in Table I for  $\text{Tb}_2\text{Ni}_2\text{In}$  and Table II for  $\text{Ho}_2\text{Ni}_2\text{In}$ , respectively. The data confirm that the crystal structure is stable down to low temperatures. The shortest interatomic distances between the  $\text{Ho}1$  atom and its nearest neighbours in  $\text{Ho}_2\text{Ni}_2\text{In}$  are listed in Table III.

TABLE III. Interatomic distances between the  $\text{Ho}1$  atom and its nearest neighbours in  $\text{Ho}_2\text{Ni}_2\text{In}$  determined from the full diffraction patterns.

distance [Å]	20.2 K	3.7 K	2.5 K	1.5 K
$\text{Ho}1\text{-Ni}2$	2.825(3)	2.815(5)	2.816(5)	2.821(4)
$\text{Ho}1\text{-Ni}1$	2.986(6)	2.99(2)	3.00(1)	2.99(1)
$\text{Ho}1\text{-In}1$	3.308(3)	3.306(5)	3.303(5)	3.299(5)
$\text{Ho}1\text{-Ho}1$	3.6715(4)	3.6648(8)	3.6660(7)	3.6652(8)
$\text{Ho}1\text{-Ho}4$	3.782(7)	3.77(1)	3.78(1)	3.79(1)
$\text{Ho}1\text{-Ho}2$	3.866(8)	3.87(2)	3.86(1)	3.85(2)

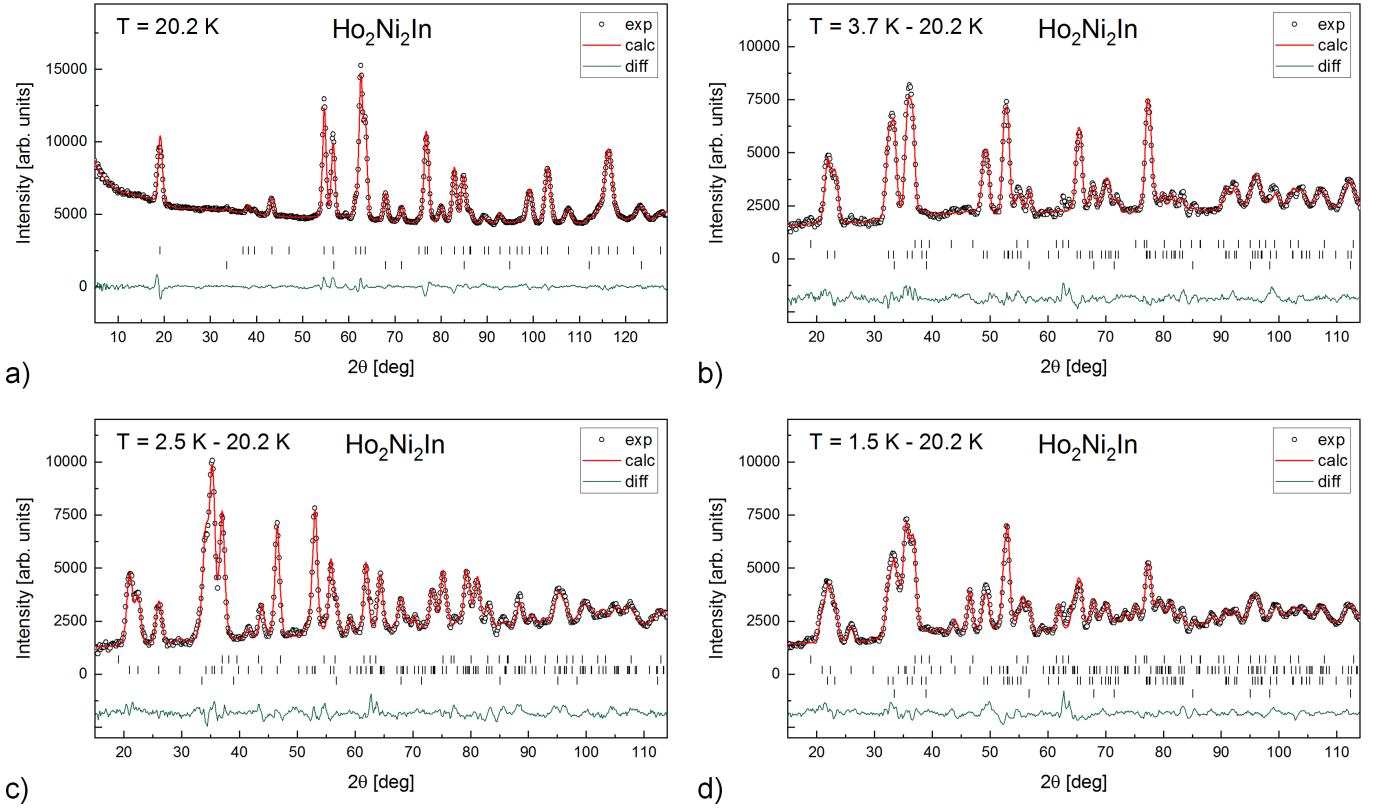


FIG. 2. Neutron diffraction patterns of  $\text{Ho}_2\text{Ni}_2\text{In}$  collected at a)  $T = 20.2$  K, b)  $T = 3.7$  K, c)  $T = 2.5$  K and d)  $T = 1.5$  K. Experimental patterns are denoted by points, while the results of Rietveld refinement by lines and the difference curves by bottom lines. From patterns b)-d), the pattern taken at  $T = 20.2$  K has been subtracted in order to obtain pure magnetic contribution. The first row of vertical bars indicates Bragg reflection positions originating from the crystal structure of  $\text{Ho}_2\text{Ni}_2\text{In}$ . The magnetic Bragg reflection positions of  $\text{Ho}_2\text{Ni}_2\text{In}$  related to the propagation vector  $\mathbf{k}_1 = [0.76, 0, 0.52]$  are denoted by the second row in b) and third row in d). The magnetic Bragg reflection positions of  $\text{Ho}_2\text{Ni}_2\text{In}$  corresponding to the propagation vectors  $\mathbf{k}_2 = [\frac{5}{6}, 0.16, \frac{1}{2}]$  and  $3\mathbf{k}_2 = [\frac{5}{2}, 0.48, \frac{3}{2}]$  are denoted by the second row in c) and d). The nuclear peak positions of  $\text{HoNi}_2$  impurity are denoted by the second row in a). The magnetic peaks from ferromagnetic order in  $\text{HoNi}_2$  are indicated by the last rows in b)-d).

Four magnetic  $R$  atoms in the  $4j$  sublattice with the local symmetry  $m2m$  are denoted as:  $R1(0, y_R, \frac{1}{2})$ ,  $R2(0, 1 - y_R, \frac{1}{2})$ ,  $R3(\frac{1}{2}, y_R + \frac{1}{2}, \frac{1}{2})$ ,  $R4(\frac{1}{2}, \frac{1}{2} - y_R, \frac{1}{2})$ . The  $R3$  and  $R4$  atom positions are related to the  $R1$  and  $R2$  ones, respectively, by the centering translation  $C = [\frac{1}{2}, \frac{1}{2}, 0]$ .

The neutron diffraction pattern of  $\text{Tb}_2\text{Ni}_2\text{In}$ , collected at 1.55 K (see Figure 1b), contains additional Bragg reflections originating from the magnetic order. These reflections can be indexed with the use of the propagation vector  $\mathbf{k} = [\frac{1}{2}, \frac{1}{2}, \frac{1}{2}]$ . The same propagation vector describes magnetic order in the isostructural  $\text{Er}_2\text{Ni}_2\text{Pb}$  compound [7]. Symmetry analysis provides four magnetic structure models related to  $\mathbf{k}$  – for details see Table II in [7]. In case of  $\text{Tb}_2\text{Ni}_2\text{In}$ , the best agreement with the experimental data ( $R_{\text{magn}} = 5.0\%$ ) is obtained for the model  $\Gamma 3$  with Tb magnetic moments equal to  $8.65(6) \mu_B$  and parallel to the  $c$ -axis. The moments follow the  $++-+$  sign sequence for the Tb1, Tb2, Tb3 and Tb4 atoms in the crystallographic unit cell, respectively. The corresponding magnetic unit cell is shown in

Figure 4. Temperature dependence of the Tb magnetic moment (see the insert in Figure 1) provides the Néel temperature equal to 40 K, which is in a good agreement with the results of macroscopic magnetic measurements [2].

Neutron diffraction patterns of  $\text{Ho}_2\text{Ni}_2\text{In}$ , collected in the 1.5-20.2 K range, are presented in Figure 5.  $\text{Ho}_2\text{Ni}_2\text{In}$  remains paramagnetic down to 9.1 K. The Bragg reflections of magnetic origin appear in the pattern collected at 8.6 K. With decreasing temperature the  $\text{Ho}_2\text{Ni}_2\text{In}$  magnetic structure undergoes two transitions visible as distinct changes in the diffraction pattern at ca. 3.5 K and ca. 2.0 K, respectively. In order to extract pure magnetic contribution, the paramagnetic pattern taken at  $T = 20.2$  K has been subtracted from the patterns recorded at lower temperatures – representative examples are shown in Figures 2b-d. Propagation vectors describing magnetic structure have been determined using the  $k$ -search computer program, while for symmetry analysis of magnetic structures the BasIreps program has been

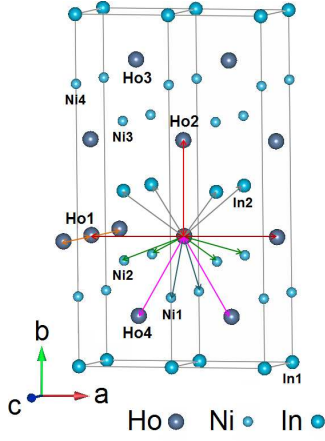


FIG. 3. Crystal unit cell of  $\text{Ho}_2\text{Ni}_2\text{In}$  (doubled along the  $a$ -axis for better visibility). The distances between the Ho1 atom and its nearest neighbours are indicated.

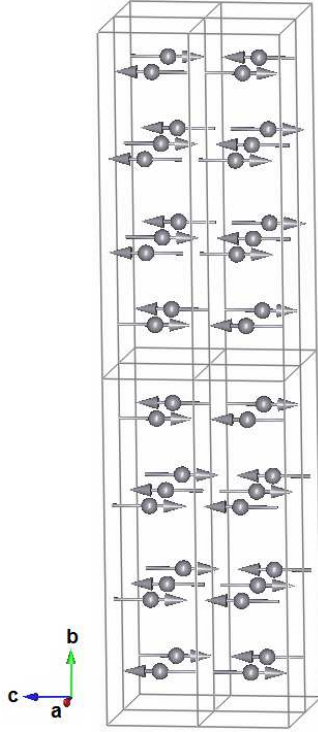


FIG. 4. Magnetic unit cell of  $\text{Tb}_2\text{Ni}_2\text{In}$ . It is doubled along three directions when compared with the crystallographic one.

utilized. Both programs are parts of the FullProf package [6]. The ferromagnetic contribution arising from the  $\text{HoNi}_2$  impurity phase has been included in all refinements performed for data collected below 13.5 K [8]. It has been assumed that all magnetic moments in  $\text{HoNi}_2$  are of the same magnitude and point at the  $[111]$  direction.

The Bragg reflections of magnetic origin, observed in

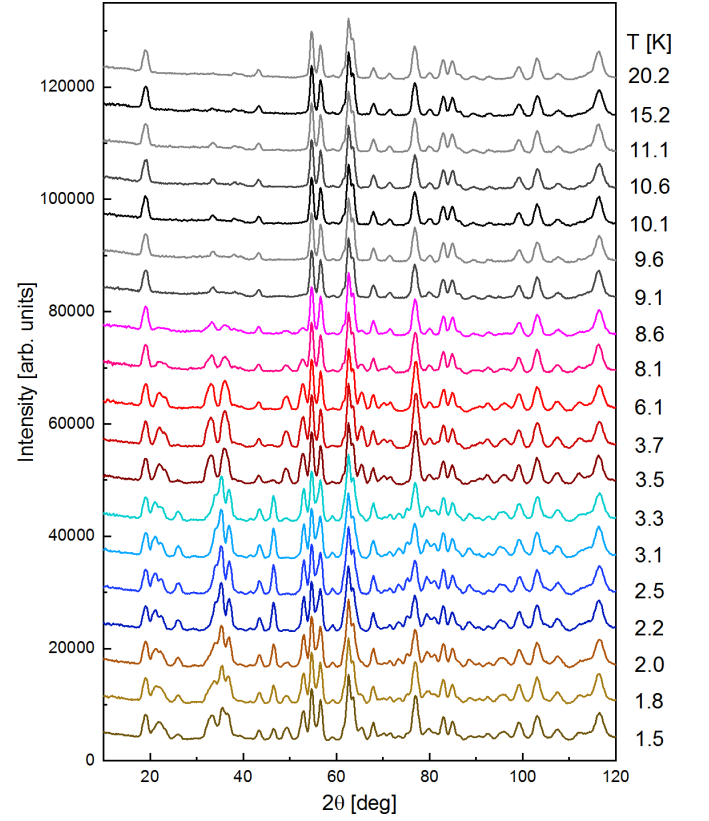


FIG. 5. Thermal evolution of neutron diffraction patterns of  $\text{Ho}_2\text{Ni}_2\text{In}$ .

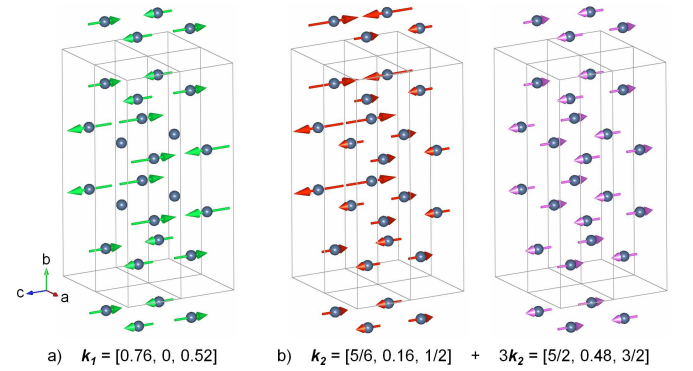


FIG. 6. Modulated magnetic structures of  $\text{Ho}_2\text{Ni}_2\text{In}$  described by the propagation vectors: a)  $\mathbf{k}_1 = [0.76, 0, 0.52]$  at  $T = 3.7$  K and b)  $\mathbf{k}_2 = [\frac{5}{6}, 0.16, \frac{1}{2}]$  and  $3\mathbf{k}_2 = [\frac{5}{2}, 0.48, \frac{3}{2}]$  at  $T = 2.5$  K.

the 3.5-8.6 K temperature range, can be indexed with an incommensurate propagation vector  $\mathbf{k}_1 = [0.76, 0, 0.52]$ . Symmetry analysis for  $\mathbf{k}_1$  and the  $4j$  Wyckoff site provides two irreducible representations: IR1 and IR2. Both representations allow for non-zero contribution to the total magnetic moments along  $a$ ,  $b$ ,  $c$  directions (Table IV). All Ho atoms belong to one orbit, therefore they are con-

TABLE IV. Magnetic structure of  $\text{Ho}_2\text{Ni}_2\text{In}$  described by the IR2 representation for the  $4j$  Wyckoff site of  $Cmmm$  space group and propagation vector  $\mathbf{k}_1 = [k_x, 0, k_z]$ .  $C_i$  coefficients denote contribution to the total magnetic moment along respective BVi basis vector,  $\mu_{tot}$  is the modulation amplitude of magnetic moment and  $R_{magn}$  is the magnetic reliability factor of the Rietveld refinement. Only the values for Ho1 and Ho2 atoms are given since Ho3 and Ho4 atoms are interrelated with them by centering translation.

$4j$	$\mathbf{k}_1 = [k_x, 0, k_z]$	IR1			IR2						
		BV1	BV2	BV3	BV1	BV2	BV3				
	Ho1										
	$(0, y_{\text{Ho}}, \frac{1}{2})$	1 0 0	0 1 0	0 0 1	1 0 0	0 1 0	0 0 1				
	Ho2										
	$(0, 1 - y_{\text{Ho}}, \frac{1}{2})$	-1 0 0	0 1 0	0 0 -1	1 0 0	0 -1 0	0 0 1				
$T$	$\text{Ho}_2\text{Ni}_2\text{In}$	$C_1$	$C_1$	$C_1$	$C_1$	$C_1$	$C_1$	$\mu_{tot}$	$k_x$	$k_z$	$R_{magn}$
[K]		$[\mu_B]$	$[\mu_B]$	$[\mu_B]$	$[\mu_B]$	$[\mu_B]$	$[\mu_B]$	$[\mu_B]$			[%]
3.7	Ho1							10.28(9)	0.7580(3)	0.5198(3)	5.3
	Ho2							10.28(9)			
1.5	Ho1							8.2(2)	0.7568(5)	0.5191(5)	5.4
	Ho2							8.2(2)			

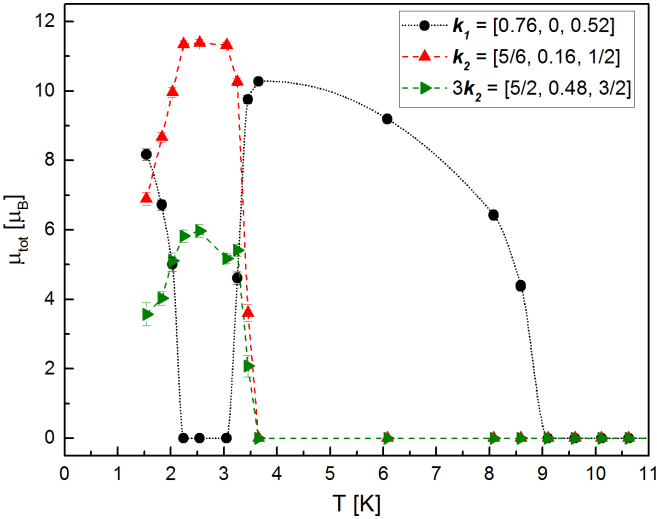


FIG. 7. Modulation amplitude of the Ho magnetic moments in  $\text{Ho}_2\text{Ni}_2\text{In}$  in function of temperature as obtained by the Rietveld refinement from difference diffraction patterns (representative fits shown in Figures 2b-d). The modulation is described either by the propagation vector  $\mathbf{k}_1 = [0.76, 0, 0.52]$  or  $\mathbf{k}_2 = [\frac{5}{6}, 0.16, \frac{1}{2}]$  and its third harmonics  $3\mathbf{k}_2 = [\frac{5}{2}, 0.48, \frac{3}{2}]$ . The lines connecting points are only guides to eye.

strained by symmetry and modulation of their magnetic moments has identical amplitude. The IR1 representation assumes parallel ordering of the  $b$ -axis components of magnetic structure and antiparallel ordering of the  $a$ - and  $c$ -axis components for the Ho1 and Ho2 atoms belonging to the same crystal unit cell. For IR2, the  $b$ -axis components are antiparallel, while the  $a$ - and  $c$ -axis ones are parallel. The results of Rietveld refinement favor the magnetic structure model related to the IR2 representation with magnetic moments oriented only along the

$c$ -axis. A representative difference pattern ( $T = 3.7$  K - 20.2 K) is presented in Figure 2b, while the corresponding magnetic structure is shown in Figure 6a. The resultant magnetic structure is antiferromagnetic. The modulation amplitude increases initially with decreasing temperature reaching  $10.3(1) \mu_B$  at  $T = 3.7$  K (see Figure 7). At the same temperature, new unindexed reflections of low intensity become visible, indicating beginning of magnetic phase transition. At  $T = 3.5$  K and 3.3 K, a co-existence of two different magnetic phases is observed. The modulation amplitude related to the  $\mathbf{k}_1 = [0.76, 0, 0.52]$  propagation vector decreases to  $9.8(2) \mu_B$  and  $4.6(2) \mu_B$  at 3.5 K and 3.3 K, respectively, and finally drops to zero at  $T = 3.1$  K.

Indexing of Bragg reflections of magnetic origin, observed between 2.2 and 3.1 K (see Figure 2c), requires two propagation vectors, namely,  $\mathbf{k}_2 = [\frac{5}{6}, 0.16, \frac{1}{2}]$  and its third harmonics,  $3\mathbf{k}_2 = [\frac{5}{2}, 0.48, \frac{3}{2}]$ , indicating that the resultant modulation of magnetic moments differs from purely sinusoidal one, observed at higher temperatures. Symmetry analysis provides identical irreducible representations (IR1 and IR2) for both  $\mathbf{k}_2$  and  $3\mathbf{k}_2$ . IR1 describes magnetic ordering within the  $ab$ -plane, while IR2 the one along the  $c$ -axis (see Table V). The Ho atoms are divided into two orbits – the first one containing the Ho1, Ho3 pair and the second one containing the Ho2, Ho4 pair. The agreement with experimental pattern is obtained for the IR2 representation (the Ho magnetic moments are parallel to the  $c$ -axis). The components of magnetic structure described by the  $\mathbf{k}_2$  propagation vector and its third harmonics  $3\mathbf{k}_2$  are visualized in Figure 6b for  $T = 2.5$  K. Although the splitting into two orbits allows for different modulation amplitudes and a phase shift between orbits, the Rietveld refinement implies identical modulation amplitudes and zero phase shift between the (Ho1, Ho3) and (Ho2, Ho4) atom pairs.



TABLE V. Magnetic structure of  $\text{Ho}_2\text{Ni}_2\text{In}$  described by the IR2 representation for the 4j Wyckoff site of  $Cmmm$  space group and propagation vectors  $\mathbf{k}_2 = [\frac{5}{6}, 0.16, \frac{1}{2}]$  and  $3\mathbf{k}_2 = [\frac{5}{2}, 0.48, \frac{3}{2}]$ .  $C_1$  coefficient is a contribution to the magnetic moment along BV1 basis vector (the first and second values apply to  $\mathbf{k}_2$  and  $3\mathbf{k}_2$ , respectively),  $\mu_{tot}$  is the modulation amplitude of magnetic moment, while  $R_{magn}$  is the magnetic reliability factor of Rietveld refinement.

		IR1		IR2			
		BV1	BV2	BV1			
	$\mathbf{k}_2 = [\frac{5}{6}, 0.16, \frac{1}{2}]$ $3\mathbf{k}_2 = [\frac{5}{2}, 0.48, \frac{3}{2}]$						
4j	Ho1 $(0, y_{Ho}, \frac{1}{2})$	1 0 0	0 1 0	0 0 1			
	Ho2 $(0, 1 - y_{Ho}, \frac{1}{2})$	1 0 0	0 1 0	0 0 1			
$T$ [K]	$\text{Ho}_2\text{Ni}_2\text{In}$	$C_1$ [ $\mu_B$ ]	$C_2$ [ $\mu_B$ ]	$C_1$ [ $\mu_B$ ]	$\mu_{tot}$ [ $\mu_B$ ]	$k_y$	$R_{magn}$ [%]
2.5	Ho1			11.41(9), 6.0(2)	11.41(9), 6.0(2)	0.1615	4.9
	Ho2			11.41(9), 6.0(2)	11.41(9), 6.0(2)		
1.5	Ho1			6.9(2), 3.5(3)	6.9(2), 3.5(3)	0.159(2)	5.9
	Ho2			6.9(2), 3.5(3)	6.9(2), 3.5(3)		

The amplitude of modulation related to the  $\mathbf{k}_2$  propagation vector equals 11.3-11.4  $\mu_B$  in the 2.2-3.1 K range, while the component related to  $3\mathbf{k}_2$  is about two times smaller and equal to 5.2-6.0  $\mu_B$  (see Figure 7). This relationship between components continues also below 2.2 K, where another magnetic phase transition occurs. It is worth noting that the magnetic structure related to  $\mathbf{k}_2$  and  $3\mathbf{k}_2$  resembles the high-temperature magnetic structure related to  $\mathbf{k}_1$  as both magnetic structures are antiferromagnetic and the magnetic moments are oriented along the  $c$ -axis.

At the lowest studied temperatures, a re-appearance of Bragg reflections of magnetic origin, indexed by the  $\mathbf{k}_1 = [0.76, 0, 0.52]$  propagation vector is observed – notice the presence of magnetic Bragg reflection at  $2\theta = 49.3^\circ$  in Figures 2b-d as well as follow thermal evolution of the  $\text{Ho}_2\text{Ni}_2\text{In}$  neutron diffraction pattern shown in Figure 5. A clear co-existence of the magnetic phase described by  $\mathbf{k}_1$  and that related to the  $\mathbf{k}_2, 3\mathbf{k}_2$  pair is visible below 2.0 K. The modulation amplitude of magnetic moments related to the  $\mathbf{k}_1$  propagation vector increases with decreasing temperature reaching finally 8.2(2)  $\mu_B$  at  $T = 1.5$  K. It exceeds the contributions related to the  $\mathbf{k}_2$  and  $3\mathbf{k}_2$  propagation vectors, which decrease at  $T = 1.5$  K to 6.9(2)  $\mu_B$  and 3.6(4)  $\mu_B$ , respectively.

In order to get more information about the nature of low-temperature magnetic phase transitions, additional heat capacity measurements have been performed in the temperature range 1.8-12 K with both increasing and decreasing temperature (see Figure 8). A lambda-shaped maximum at 9.0 K is typical of the second-order transition from antiferro- to paramagnetic state, while a distinct thermal hysteresis visible in the temperature range 2.5-3.5 K (see the insert in Figure 8) is characteristic of the first-order transition and coincides with the transition temperature between the magnetic phase described by the  $\mathbf{k}_1$  propagation vector and that related to the  $\mathbf{k}_2$  and  $3\mathbf{k}_2$  vector pair.

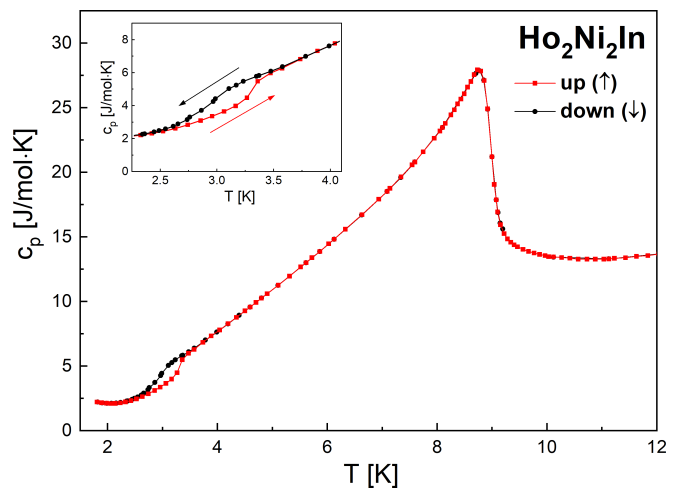


FIG. 8. Temperature dependence of the molar heat capacity of  $\text{Ho}_2\text{Ni}_2\text{In}$  in the temperature range 1.8-12.0 K. The insert shows the low-temperature data with increasing (up) an decreasing (down) temperature. The lines are guides for the eye.

#### IV. DISCUSSION

Analysis of the X-ray diffraction pattern as well as nuclear contribution to the neutron diffraction pattern in function of temperature indicates that the orthorhombic crystal structure is stable in a broad temperature range including the magnetically ordered state (see Tables I and II). The crystal structure is highly anisotropic with the  $b$  lattice constant more than three times larger than the  $a$  and  $c$  ones (see Figure 3). The structure consists of the  $ac$ -planes of various kinds stacked along the  $b$ -axis direction, namely, the  $R$  atoms planes are intercalated between the Ni- and In-planes following the sequence: In-R-Ni-Ni-R-In-R-Ni-Ni-R-In. The shortest distances between the Ho atoms within the  $ac$ -plane and those located

at different planes differ (see Table III) – the lowest are found along the  $c$ -axis which is the direction of magnetic moment in the ordered state.

The results reported in this work indicate different kinds of collinear antiferromagnetic orderings present in the investigated compounds, namely, a commensurate one in  $\text{Tb}_2\text{Ni}_2\text{In}$  and an incommensurate one in  $\text{Ho}_2\text{Ni}_2\text{In}$ . In  $\text{Tb}_2\text{Ni}_2\text{In}$ , the low-temperature magnetic structure is described by the propagation vector  $\mathbf{k} = [\frac{1}{2}, \frac{1}{2}, \frac{1}{2}]$ , leading to a magnetic unit cell that has the lattice parameters doubled with respect to the crystallographic cell along all three principal crystallographic directions (see Figure 4). In  $\text{Ho}_2\text{Ni}_2\text{In}$ , a sequence of incommensurate modulated magnetic structures appears with decreasing temperature. Below 9 K a magnetic structure related to  $\mathbf{k}_1 = [0.76, 0, 0.52]$  is observed, while in the temperature range 2.2 and 3.1 K two propagation vectors ( $\mathbf{k}_2 = [\frac{5}{6}, 0.16, \frac{1}{2}]$  and  $3\mathbf{k}_2$ ) are required to describe the magnetic structure. Finally, below 2 K a coexistence of both above mentioned magnetic structures is detected.

Temperature-induced transformations of magnetic structures have been found in a number of intermetallic compounds (see Table 1 in [9]). Such transformations of the magnetic structure can be understood on the basis of a realistic mean-field model, which takes into account both periodic-change-field and crystal electric field effects [9]. A sequence of magnetic structures similar to those reported in this work for  $\text{Ho}_2\text{Ni}_2\text{In}$  has been previously observed for  $\text{UNi}_2\text{Si}_2$  [10]. With decreasing temperature, an incommensurate modulated magnetic structure ( $\mathbf{k} = [0, 0, 0.745]$ ) transforms into an intermediate simple antiferromagnetic one, and finally again to a modulated one ( $\mathbf{k} = [0, 0, \frac{2}{3}]$ ) with a ferromagnetic component. Such an evolution of magnetic structure has been interpreted on the basis of the Heisenberg model with biquadratic exchange [11].

The magnetic moments in  $\text{Tb}_2\text{Ni}_2\text{In}$  and  $\text{Ho}_2\text{Ni}_2\text{In}$  are parallel to the  $c$ -axis, while they are parallel to the  $b$ -axis in  $R_2\text{Ni}_2\text{In}$  ( $R = \text{Er}$  and  $\text{Tm}$ ) [5]. Such a change of orientation of the magnetic moment with increasing number of the  $4f$  electrons can be attributed to change of sign of the Stevens operator  $\alpha_J$  which is negative for Tb and Ho and positive for Er and Tm [12].

In both compound the  $R$ - $R$  interatomic distances are about 3.7 Å and therefore they are larger than the sum of respective  $R^{3+}$  ionic radii. Such a result suggest presence of indirect exchange interactions of the RKKY-type. The RKKY model predicts proportionality between the Néel temperature and the de Gennes factor defined as  $(g_J - 1)^2 J(J + 1)$ , where  $g_J$  is a Landé splitting factor and  $J$  is a total angular momentum of the corresponding magnetic ion [13]. Figure 11 in [2] shows a comparison between the experimentally determined Néel temperatures for  $R_2\text{Ni}_2\text{In}$  ( $R = \text{Gd-Tm}$ ) and those calculated according the RKKY theory. A large discrepancy

between the experimental and calculated temperatures for  $\text{Tb}_2\text{Ni}_2\text{In}$  indicates a strong influence of the crystalline electric field (CEF) on magnetic state formation [14]. Therefore the magnetic structures in  $R_2\text{Ni}_2\text{In}$  ( $R$  - rare earth element) result from competition between the RKKY- and CEF-type interactions. Such a competition may lead to complex magnetic properties including temperature-induced magnetic order-order transitions [15]. It is worth noting that such transitions have been observed also in the isostructural  $R_2\text{Ni}_2\text{Pb}$  ( $R = \text{Ho}, \text{Er}$ ) compounds [7, 16]. In  $\text{Ho}_2\text{Ni}_2\text{Pb}$ , a sine-modulated commensurate magnetic order described by the magnetic unit cell  $5a \times b \times c$  develops below  $T_N = 7$  K. The magnetic structure turns into square-modulated one below  $T_t = 3$  K. In  $\text{Er}_2\text{Ni}_2\text{Pb}$ , an incommensurate modulated magnetic structure ( $\mathbf{k} = [0.8409(1), 0, \frac{1}{2}]$ ) has been detected below  $T_N = 3.5$  K. With decreasing temperature, two intermediate incommensurate magnetic phases, related to the  $[0.5973(1), 0, \frac{1}{2}]$  and  $[0.5330(3), 0, \frac{1}{2}]$  propagation vectors, respectively, appears. A commensurate magnetic structure, involving two propagation vectors ( $[\frac{1}{2}, \frac{1}{2}, \frac{1}{2}]$  and  $[0, 0, \frac{1}{2}]$ ), is found as magnetic ground state.

## V. SUMMARY AND CONCLUSIONS

The results presented in this work confirm that the crystal structure of ternary  $R_2\text{Ni}_2\text{In}$  ( $R = \text{Tb}$  and  $\text{Ho}$ ) is orthorhombic of the  $\text{Mn}_2\text{AlB}_2$ -type (space group  $Cmmm$ ) in both paramagnetic and magnetically ordered states. At low temperatures the rare earth magnetic moments are found to order antiferromagnetically with the rare earth magnetic moments being parallel to the  $c$ -axis. In  $\text{Tb}_2\text{Ni}_2\text{In}$ , a commensurate ( $\mathbf{k} = [\frac{1}{2}, \frac{1}{2}, \frac{1}{2}]$ ) collinear antiferromagnetic structure with is formed below  $T_N = 40$  K. In  $\text{Ho}_2\text{Ni}_2\text{In}$ , a sequence of order-order magnetic transitions is observed. An incommensurate antiferromagnetic sine-modulated structure, related to  $\mathbf{k}_1 = [0.76, 0, 0.52]$ , is detected below  $T_N = 9$  K. The structure turns around 3 K into another incommensurate one, which is described by two different propagation vectors, namely,  $\mathbf{k}_2 = [\frac{5}{6}, 0.16, \frac{1}{2}]$  and  $3\mathbf{k}_2$ . Below 2 K the structure related to  $\mathbf{k}_1$  reappears and a coexistence of both above mentioned magnetic structures is observed. Heat capacity data reveal that the transition at 3 K is of the first-order type.

## ACKNOWLEDGEMENTS

Kind hospitality and financial support extended to two of us (S. B. and A. S.) by the Helmholtz-Zentrum Berlin für Materialien und Energie (HZB) is gratefully acknowledged.

- 
- [1] V. I. Zaremba, V. A. Bruskov, P. Yu. Zavali, Ya. M. Kalychak, Crystal structure of  $R_2\text{Ni}_2\text{In}$  compounds ( $R = \text{Y}, \text{Sm}, \text{Gd}, \text{Tb}, \text{Ho}, \text{Er}, \text{Tm}, \text{Lu}$ ), *Izv. Akad. Nauk SSSR, Neorg. Mater.* 24 (1988) 409–411 (Engl. transl.: *Inorg. Mater.* 24 (1988) 330–332).
- [2] A. Szytuła, S. Baran, J. Przewoźnik, Yu. Tyvanchuk, Ya. Kalychak, Magnetic properties and specific heat of  $R_2\text{Ni}_2\text{In}$  ( $R = \text{Gd–Tm}$ ) compounds, *J. Magn. Magn. Mater.* 387 (2015) 83–89. doi:10.1016/j.jmmm.2015.03.084.
- [3] Z. Zhang, P. Wang, H. Rong, L. Li, Structural and cryogenic magnetic properties of  $RE_2\text{Ni}_2\text{In}$  ( $RE = \text{Pr}, \text{Nd}, \text{Dy}$  and  $\text{Ho}$ ) compounds, *Dalton Trans.* 48 (2019) 17792–17799. doi:10.1039/c9dt03245b.
- [4] A. Szytuła, S. Baran, A. Hoser, Ya. M. Kalychak, B. Penc, Yu. Tyvanchuk, Neutron diffraction studies of  $\text{Tb}_2\text{Ni}_{2-x}\text{In}$  intermetallic compounds, *Acta Phys. Pol. A* 124 (2013) 994–997. doi:10.12693/APhysPolA.124.994.
- [5] S. Baran, A. Szytuła, A. Hoser, Collinear antiferromagnetic structure in  $R_2\text{Ni}_2\text{In}$  ( $R = \text{Er}, \text{Tm}$ ), *J. Alloys Compd.* 696 (2017) 1278–1281. doi:10.1016/j.jallcom.2016.12.072.
- [6] J. Rodríguez-Carvajal, Recent developments of the program fullprof, *Newsletter of the Commission for Powder Diffraction of the IUCr* 26 (2001) 12–19.
- [7] K. Prokeš, E. Muñoz-Sandoval, A. D. Chinchure, J. A. Mydosh, Competing magnetic structures and magnetic transitions in  $\text{Er}_2\text{Ni}_2\text{Pb}$ : Powder neutron diffraction measurements, *Phys. Rev. B* 78 (2008) 014425. doi:10.1103/PhysRevB.78.014425.
- [8] J. Ćwik, Y. Koshkid'ko, K. Nenkov, E. A. Tereshina, K. Rogacki, Structural, magnetic and magnetocaloric properties of  $\text{HoNi}_2$  and  $\text{ErNi}_2$  compounds ordered at low temperatures, *J. Alloys Compd.* 735 (2018) 1088–1095. doi:10.1016/j.jallcom.2017.11.194.
- [9] D. Gignoux, D. Schmitt, Competition between commensurate and incommensurate phases in rare-earth systems: Effects on  $H-T$  magnetic phase diagrams, *Phys. Rev. B* 48 (1993) 12682–12691. doi:10.1103/PhysRevB.48.12682.
- [10] H. Lin, L. Rebelsky, M. F. Collins, J. D. Garrett, W. J. L. Buyers, Magnetic structure of  $\text{uni}_2\text{Si}_2$ , *Phys. Rev. B* 43 (1991) 13232–13239. doi:10.1103/PhysRevB.43.13232.
- [11] A. Mailhot, M. L. Plumer, A. Caillé, P. Azaria, Effect of biquadratic exchange on the axial heisenberg model: Application to the magnetic phase transitions in  $\text{uni}_2\text{Si}_2$ , *Phys. Rev. B* 45 (1992) 10399–10407. doi:10.1103/PhysRevB.45.10399.
- [12] K. W. H. Stevens, Matrix elements and operator equivalents connected with the magnetic properties of rare earth ions, *Proc. Phys. Soc. A* 65 (1952) 209–215. doi:10.1088/0370-1298/65/3/308.
- [13] P. G. D. Gennes, Interactions indirectes entre couches 4f dans les métaux de terres rares, *J. Phys. Radium* 23 (1962) 510–521. doi:10.1051/jphysrad:01962002308-9051001.
- [14] D. R. Noakes, G. K. Shenoy, The effect of a crystalline electric field on the magnetic transition temperatures of rare-earth rhodium borides, *Phys. Lett. A* 91 (1982) 35–36. doi:10.1016/0375-9601(82)90258-4.
- [15] J. Rossat-Mignod, Magnetic structures, in: K. Sköld, D. L. Price (Eds.), *Methods in Experimental Physics*, volume 23, Elsevier, San Diego, 1987, pp. 69–157.
- [16] K. Prokeš, E. Muñoz-Sandoval, A. D. Chinchure, J. A. Mydosh, Uncompensated antiferromagnetic structure of  $\text{Ho}_2\text{Ni}_2\text{Pb}$ , *Eur. Phys. J. B* 43 (2005) 163–174. doi:10.1140/epjb/e2005-00039-1.